2024 IEEE International Conference on Robotics and Automation (ICRA 2024)
May 13-17, 2024. Yokohama, Japan

An Integrated Position-velocity-force Method for Safety-enhanced Shared Control in Robot-assisted Surgical Cutting*

Xilin Xiao, Xiaojian Li, Yudong Shi, Jin Fang, Lin Li, Pengfei He, Hangjie Mo

Abstract— **Numerous studies have emphasized the application of autonomous intelligence in human-robot shared control to enhance surgical convenience and efficiency. However, the neglect of human dominance may reduce surgical safety. This paper developed a safety-enhanced human-robot shared control method by intelligently allocating control authority, with the surgeon remaining the leader during the surgical procedure. Three controllers are designed initially, including a master hand position (MP) controller and a master hand velocity (MV) controller related to the surgeon's manipulation, and a planned trajectory tracking (PT) controller related to the robot. In precision surgical manipulation scenarios, precise tracking of the human's operation is achieved by combining MP and MV controllers, while a combination of MV and PT controllers is developed in high-efficiency surgical scenarios, which relaxes the requirement for precise tracking of hand position and enables precise robot assistance guided by the velocity of human hand. The autonomous scenarios and controllers switching are accomplished through a motion fusion mechanism, which is achieved via optimizing evaluation functions that are reliant on future states. Furthermore, a force feedback mechanism is proposed to help human understand the intent of autonomous control to improve safety. The feasibility and effectiveness of this method have been validated through simulations and experiments.**

Keywords: surgical robot, shared control, motion fusion, safety-enhanced, force feedback

I. INTRODUCTION

In most current clinical applications, robot-assisted minimally invasive surgery (RMIS) is dominated by the master-slave system, such as da Vinci Surgical Robot. Before the advent of fully autonomous surgery [1], shared control[2] shows great application potential for intelligent surgical assistance by fusing human intelligence with autonomous algorithms to improve surgical quality [3]. Earlier scholars[4, 5] have emphasized that the design of human-robot shared control should prioritize human-centeredness and adhere to the principles of convenience, controllability, safety, transparency, and adaptability.

This work is fully supported by the National Natural Science Foundation of China (62133004, 72293585 and 72188101), the Anhui Provincial Natural Science Foundation (2108085J33), and the Anhui Provincial Major Science and Technology Project (202203a05020010), the Fundamental Research Funds for the Central Universities (JZ2022HGPA0311 and JZ2023HGQA0125) (*corresponding author: Hangjie Mo, email: mohj@hfut.edu.cn).

The authors are with the School of Management, Hefei University of Technology, Hefei, China and the Key Laboratory of Process Optimization and Intelligent Decision-Making, Hefei University of Technology, Hefei, China (email: xxl168wk@mail.hfut.edu.cn; lixj90@hfut.edu.cn; shiyudong@mail.hfut.edu.cn;fangjin@mail.hfut.edu.cn;cynerelee@hfut.edu.cn;2019010098@mail.hfut.edu.cn;mohj@hfut.edu.cn).

In the early stages, scholars sought to enhance the convenience of surgical operations by developing various shared control methods tailored to specific scenarios, compensating for periodic physiological movements. For instance, compensating for hand tremors [6], heart beating [7-9], and respiratory movement [10]. Then, to further explore the potential applications of shared control and enhance surgical safety and quality, a number of studies have focused on virtual fixtures [11] or other force interaction methods [12-14], such as organ protection [15], target guidance [16-22] and obstacle avoidance [23-25]. However, due to the limited intelligence, these methods face challenges in dynamically and flexibly adapting to changes in human control behavior.

Furthermore, some scholars focused on the arbitration law to combine human intelligence with autonomous algorithms [26-29]. Saeidi, Opfermann et al.[27] developed a "self-aware" confidence based shared control strategy for control allocation between human and robot, which triggers the weight transfer based on the information of the acquired image. Franceschi, Pedrocchi et al.[29] through the dynamic interaction force imposed by human to manage the leader-follower transition based on a Cooperative Game theory method. Zhang, Wu et al.[30] proposed a role adaptation mechanism that according to the surgical operation contexts predicted by a neural network model. Although these methods consider the integration of autonomous robot control and human control, they have placed excessive emphasis on the utilization of autonomous intelligence while neglecting the human dominance in surgery. In other words, if autonomous intelligence takes on as a leader, there is a risk of system delay that can impact timely human intervention when the surgeon becomes aware of an impending danger.

Overall, current researches for human-robot shared control often emphasize the use of autonomous intelligence, sometimes neglecting the importance of system controllability and the potential safety risks associated with transferring control between the human and the robot. In response to this oversight, we have proposed a safety-enchanced shared control approach. The principal contributions of this paper can be delineated as follows:

(1) Through the judicious design and integration of the MP, MV, and PT controllers, the proposed control method ensures the surgeon's sustained leadership throughout the surgical procedure, thereby bolstering the safety of Human-Robot Interaction.

(2) An intricate fusion motion mechanism has been developed to facilitate intelligent and dynamic control authority allocation between the MP, MV, and PT controllers. This mechanism is realized by optimizing evaluation functions predicated upon anticipated states.

(3) A force feedback mechanism has been developed to assist the surgeon in discerning the divergence between human hand actual position and the motion fusion control output. This refinement seeks to bolster the safety of the shared control system.

II. Problem Statement

This paper takes the surgical cutting task as an example. As shown in Fig. 1, a surgical cutting trajectory is predefined based on the surgeon's experience, called planned trajectory. A guiding channel is further defined as human-robot shared control workspace according to the planned trajectory. Within this range, the surgeon can seek assistance from the robot to achieve efficient and precise cutting. The blue line denotes the trajectory that is generated by the surgeon during surgical procedure through the control of the master console. During the surgical cutting procedure, myriad factors merit attention. In certain instances, robotic assistance can enable the surgeon to achieve an exact cutting trajectory tailored to their requirements or circumvent erroneous maneuvers. Under these circumstances, the desired fusion trajectory should align closely with the planned path. Conversely, there are scenarios where the surgeon's control is paramount for actively adjusting the cutting trajectory — for example, during electric coagulation hemostasis, obstacle evasion, emergency halts, and deliberate cessation of the cutting process. In these situations, the ideal fusion trajectory should mirror the surgeon's operational path. Consequently, the desired fusion trajectory is depicted as a green line in Fig. 1. It is seen that the robot's guidance can effectively mitigate both hand tremors and aberrant actions. Moreover, active hand control signals, such as obstacle avoidance, robot assistance pause and active termination, are discernible and strictly executed by surgical robot, ensuring alignment with the surgeon's operative trajectory.

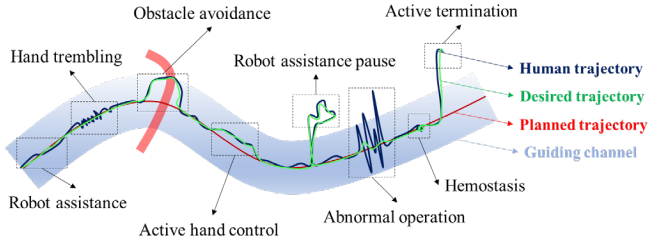

Fig. 1: The detailed operations in the robotic surgical cutting task

For the aforementioned surgical cutting procedure, relying solely on sensor data or a predefined threshold for achieving weight transfer between the human and robot may compromise the system's adaptability to the diverse operational demands of the surgeon. Furthermore, a complete weight transition or alternating leadership roles between the human and robot could risk depriving the surgeon of control authority during the operation. Such interaction modalities might impede surgeons from executing certain proactive tasks, subsequently diminishing the surgery's safety and controllability. To cater to the adaptability of human-robot interactions within the surgical environment and the diverse nuances of human operations, it is imperative to devise a human-led shared control methodology to improve the safety of surgical procedures.

III. Methodology

The safety-enhanced shared control method we propose is depicted in Fig. 2. It encompasses the following components: initial controller design, a motion fusion mechanism, a predictive evaluation and optimization model, and a force feedback mechanism. Both human and robotic control objectives are taken into account, which are divided into a master hand position (MP) tracking objective, a master hand velocity (MV) tracking objective and a planned trajectory tracking (PT) tracking objective.

Firstly, three controllers are designed, including a MP controller and a MV controller related to the surgeon's manipulation, and a PT controller related to the robot autonomous trajectory. The MP controller is designed to track the position signal generated by the human's operation of the master console. The MV controller aims to track the velocity signal when human operates the master console. Meanwhile, the PT controller is focused on tracking the planned trajectory. Secondly, a predictive evaluation optimization model is designed to improve the performance of each controller and balance the authority allocation of each controller in different scenarios. And a penalty mechanism is introduced to affect the evaluation function of the MP controller and the PT controller, and to accomplish the switch between different autonomous scenarios and controllers. Furthermore, during the real-time motion fusion control phase, the initially designed controllers' inputs and the evaluation function gradient of each controller are fused based on the gradient in the global weighting. Finally, a master force interface is constructed to provide feedback on the discrepancy between human hand actual position and the motion fusion control output.

In this study, we first establish a virtual mass-spring-damper system to ensure the continuity of the surgical instrument tip's trajectory, expressed as:

$$\begin{bmatrix}\dot{\boldsymbol{x}}\\ \ddot{\boldsymbol{x}}\end{bmatrix}=\begin{bmatrix}0 & 1\\ -\frac{k}{m} & -\frac{b}{m}\end{bmatrix}\begin{bmatrix}\boldsymbol{x}\\ \dot{\boldsymbol{x}}\end{bmatrix}+\begin{bmatrix}0\\ \frac{1}{m}\end{bmatrix}[\boldsymbol{u}] \tag{1}$$

where $\boldsymbol{x}$ represents the Cartesian space coordinate of the surgical instrument tip, anchored to a 6-degree-of-freedom manipulator, and is defined as the state vector, $\boldsymbol{u}$ is the fusion control input vector by fusing the aforementioned three controllers and the evaluation function gradient values of three controllers, $\dot{\boldsymbol{x}}$ is the velocity vector of state, $\ddot{\boldsymbol{x}}$ is the acceleration vector of state, m, b, and k denote the inertia, damping, and stiffness parameters of the spring-mass-damper system, respectively.

The state $\boldsymbol{x}$ related to the instrument tip is further transform to the state $\boldsymbol{X}$, which is Cartesian space coordinate of the robot end-effector under the remote center of motion (RCM) constraint. Finally, the state representation of $\boldsymbol{\theta}$ in the joint space of a robot is obtained by Jacobian matrix operation, so the joint speed $\dot{\boldsymbol{\theta}} \in \mathbb{R}^6$ can be defined:

$$\dot{\boldsymbol{\theta}} = \boldsymbol{J}^{-1}(\boldsymbol{\theta})\dot{\boldsymbol{X}} \tag{2}$$

where $\boldsymbol{J}^{-1}(\boldsymbol{\theta})$ represents Jacobian matrix from joint space to Cartesian space, and $\dot{\boldsymbol{X}}$ represents the velocity of the robot's end-effector velocity in Cartesian space.

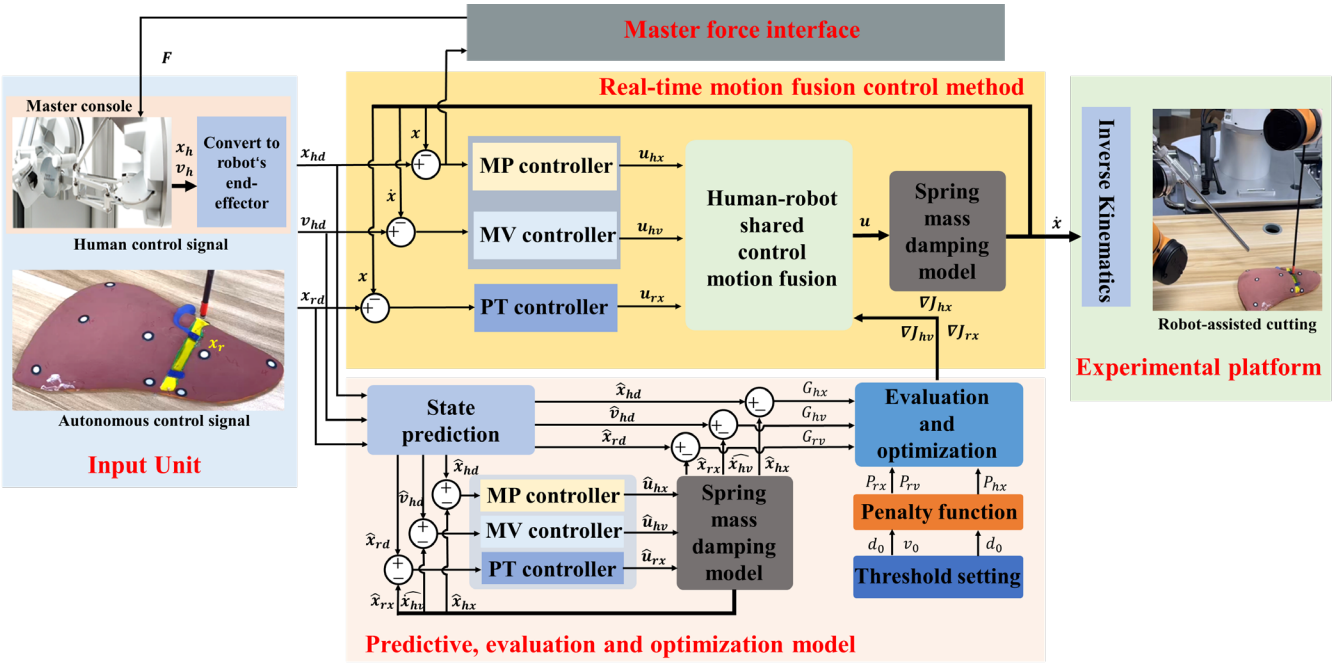

Fig. 2: The framework of the safety-enhanced human-robot shared control method

A. Initial controller design

Consider the tissue electrocoagulation cutting of a minimally invasive surgical robot defined in section 2, three control objectives are defined as $\boldsymbol{x_{hd}}$, $\boldsymbol{v_{hd}}$ and $\boldsymbol{x_{rd}}$, and calculated by the master hand position $\boldsymbol{x_h}$, the master hand velocity $\boldsymbol{v_h}$ and the planned trajectory $\boldsymbol{x_r}$, respectively. According to the three control objectives, three feedback controllers are designed based on system (1).

(1) MP Controller Design

The MP controller $\boldsymbol{u_{hx}}$ is simply designed as follows:

$$\boldsymbol{u_{hx}} = k_{px}\boldsymbol{e_{hx}} + k_{dx}\dot{\boldsymbol{e}}_{\boldsymbol{hx}} \tag{3}$$

$$\boldsymbol{e_{hx}} = \boldsymbol{x_{hd}} - \boldsymbol{x} \tag{4}$$

where k_{px} and k_{dx} are the corresponding parameters of PD control method, $\boldsymbol{e_{hx}}$ represents the error between the desired position of the MP controller and the final state.

(2) MV Controller Design

The velocity tracking controller $\boldsymbol{u_{hv}}$ is deliberately designed to be imprecise, which is just to obtain the movement trend of the human hand.

$$\boldsymbol{u_{hv}} = k_{pv}\boldsymbol{e_{hv}} \tag{5}$$

$$\boldsymbol{e_{hv}} = \boldsymbol{v_{hd}} - \dot{\boldsymbol{x}} \tag{6}$$

where k_{pv} is the corresponding parameters of P control method, $\boldsymbol{e_{hv}}$ represents the error between the desired velocity of MV controller and the velocity vector of state.

(3) PT Controller Design

The PT controller $\boldsymbol{u_{rx}}$ is simply designed as follows:

$$\boldsymbol{u_{rx}} = k_{pr}\boldsymbol{e_{rx}} + k_{dr}\dot{\boldsymbol{e}}_{\boldsymbol{rx}} \tag{7}$$

$$\boldsymbol{e_{rx}} = \boldsymbol{x_{rd}} - \boldsymbol{x} \tag{8}$$

where k_{pr} and k_{dr} are the corresponding parameters of PD control method, $\boldsymbol{e_{rx}}$ represents the error between the desired position of the PT controller and the final state.

B. Predictive evaluation and optimization

The effect of each control strategy is evaluated by using the evaluation function. The whole evaluation processes are established by system (1) and use a prediction model with fixed prediction horizon[31] to obtain the future states of three control objectives $\hat{\boldsymbol{x}}_{\boldsymbol{hd}}$, $\hat{\boldsymbol{v}}_{\boldsymbol{hd}}$ and $\hat{\boldsymbol{x}}_{\boldsymbol{rd}}$. The gradient optimization function is used to improve the performance of each simply initial designed controller and to allocate control authority between three controllers. The penalty function is introduced to limit the effects of MP or PT controllers, by reducing the values of the evaluation function to zeros. Therefore, the autonomous scenarios switching between the precision surgical manipulation scenario and the high-efficiency surgical scenario can be accomplished.

(1) MP evaluation function

The MP evaluation function (9) is derived to evaluate the MP controller effectiveness during the prediction period T.

$$J_{hx} = \int_{t_0}^{t_0+T} max(0, G_{hx}(\boldsymbol{x}_0, \hat{\boldsymbol{x}}_{\boldsymbol{hx}}, \hat{\boldsymbol{x}}_{\boldsymbol{hd}}) - P_{hx}(\boldsymbol{v_{hd}}, v_0))dt \tag{9}$$

$$G_{hx} = \|\hat{\boldsymbol{x}}_{\boldsymbol{hd}} - \hat{\boldsymbol{x}}_{\boldsymbol{hx}}\|^2 \tag{10}$$

$$P_{hx} = max(0, \|\boldsymbol{v_{hd}}\| - v_0)^2 \tag{11}$$

$$\boldsymbol{\nabla J_{hx}} = \frac{\partial J_{hx}}{\partial x}|_{\boldsymbol{x=x_0}} \tag{12}$$

where J_{hx} represents the accumulated evaluation value of MP at time t_0. G_{hx} is the evaluation value of MP at time t in the prediction period, $\hat{\boldsymbol{x}}_{\boldsymbol{hx}}$ denotes the system state under the MP controller action during the prediction period T, P_{hx} is the penalty function designed to reduce J_{hx} to zero when $\|\boldsymbol{v_{hd}}\| > v_0$, thereby limiting the effect of controller MP. v_0

is the velocity threshold to trigger the penalty function P_{hx}. $\boldsymbol{x}_0$ is the system state at time t_0. $\boldsymbol{\nabla J_{hx}}$ is the evaluation gradient of the MP controller.

(2) MV evaluation function

The MV evaluation function (13) is derived to evaluate the MV controller effectiveness during the prediction period T.

$$J_{hv} = \int_{t_0}^{t_0+T} G_{hv}(\boldsymbol{x}_0, \widehat{\boldsymbol{v}}_{\boldsymbol{hd}}, \widehat{\boldsymbol{x}}_{\boldsymbol{hv}})dt \tag{13}$$

$$G_{hv} = \left\|\widehat{\boldsymbol{v}}_{\boldsymbol{hd}} - \widehat{\boldsymbol{x}}_{\boldsymbol{hv}}\right\|^2 \tag{14}$$

$$\boldsymbol{\nabla J_{hv}} = \frac{\partial J_{hv}}{\partial \boldsymbol{x}}|_{\boldsymbol{x}=\boldsymbol{x_0}} \tag{15}$$

where J_{hv} represents the accumulated evaluation value of MV at time t_0, G_{hv} is the evaluation value of MV at time t during the prediction period, $\widehat{\boldsymbol{x}}_{\boldsymbol{hv}}$ denotes the system velocity under the MV controller action in the prediction period T, $\widehat{\boldsymbol{v}}_{\boldsymbol{hd}}$ is the predicted future state of MV control objective. $\boldsymbol{\nabla J_{hv}}$ is the evaluation gradient of the MV controller.

(3) PT evaluation function

The PT evaluation function (16) is defined to evaluate the PT controller effectiveness during the prediction period T.

$$J_{rx} = \int_{t_0}^{t_0+T} max(0, G_{rx}(\boldsymbol{x}_0, \widehat{\boldsymbol{x}}_{\boldsymbol{rx}}, \widehat{\boldsymbol{x}}_{\boldsymbol{rd}}) - P_{rx}(\boldsymbol{x}_0, \widehat{\boldsymbol{x}}_{\boldsymbol{rd}}, d_0) - P_{rv}(v_0, \boldsymbol{v}_{\boldsymbol{hd}}))dt \tag{16}$$

$$G_{rx} = \|\widehat{\boldsymbol{x}}_{\boldsymbol{rd}} - \widehat{\boldsymbol{x}}_{\boldsymbol{rx}}\|^2 \tag{17}$$

$$P_{rx} = max(0, \|\boldsymbol{x}_{\boldsymbol{0}} - \widehat{\boldsymbol{x}}_{\boldsymbol{rd}}\| - d_0)^2 \tag{18}$$

$$P_{rv} = max(0, v_0 - \|\boldsymbol{v}_{\boldsymbol{hd}}\|)^2 \tag{19}$$

$$\boldsymbol{\nabla J_{rx}} = \frac{\partial J_{rx}}{\partial \boldsymbol{x}}|_{\boldsymbol{x}=\boldsymbol{x_0}} \tag{20}$$

where J_{rx} is the accumulated evaluation value of PT at time t_0, G_{rx} is the evaluation value of PT at time t during the prediction period, $\widehat{\boldsymbol{x}}_{\boldsymbol{rx}}$ is the system state under the PT controller action in the prediction period T, $\widehat{\boldsymbol{x}}_{\boldsymbol{rd}}$ is the predicted future state of PT objective. P_{rx} is the penalty function designed to reduce J_{rx} to zero when the system trajectory deviates from the guiding channel $\|\boldsymbol{x}_{\boldsymbol{0}} - \widehat{\boldsymbol{x}}_{\boldsymbol{rd}}\|^2 > d_0$, P_{rv} is the penalty function designed to reduce J_{rx} to zero when $\|\boldsymbol{v}_{\boldsymbol{hd}}\| < v_0$. d_0 is the radius of the guiding channel.

C. Motion fusion method

To balance the authority allocation of each controller in different scenarios, the motion fusion method is used to find an optimal solution by fusing the inputs of each controller and evaluation gradient of each controller:

$$\boldsymbol{u} = \frac{||\boldsymbol{\nabla J_{hx}}||}{||\boldsymbol{\nabla J}||}\boldsymbol{u_{hx}} + \frac{||\boldsymbol{\nabla J_{hv}}||}{||\boldsymbol{\nabla J}||}\boldsymbol{u_{hv}} + \frac{||\boldsymbol{\nabla J_{rx}}||}{||\boldsymbol{\nabla J}||}\boldsymbol{u_{rx}} - \lambda \boldsymbol{K_o}\varphi_\alpha(\boldsymbol{\nabla J}) \tag{21}$$

$$\boldsymbol{\nabla J} = \boldsymbol{\nabla J_{hx}} + \boldsymbol{\nabla J_{hv}} + \boldsymbol{\nabla J_{rx}} \tag{22}$$

$$\varphi_\alpha(\boldsymbol{\nabla J}) = \begin{cases} \alpha \boldsymbol{\nabla J}/\|\boldsymbol{\nabla J}\|, & \|\boldsymbol{\nabla J}\| > \alpha \\ \boldsymbol{\nabla J}, & \|\boldsymbol{\nabla J}\| \le \alpha \end{cases} \tag{23}$$

where $\boldsymbol{K_o}$ represents the proportionality coefficient matrix, $\boldsymbol{\nabla J}$ denotes the accumulated gradient of three controllers, λ is the step size of gradient, $\varphi_\alpha(\cdot)$ is the saturation suppression function, α is a threshold constant designed to avoid system instability caused by excessive gradient value.

D. Force feedback

The force feedback scheme is designed to give the surgeon intuitive tactile sensation and enhance safety:

$$F = k_f \boldsymbol{e_f} + b_f \dot{\boldsymbol{e}}_{\boldsymbol{f}} + m_f \ddot{\boldsymbol{e}}_{\boldsymbol{f}} \tag{24}$$

$$\boldsymbol{e_f} = \boldsymbol{x} - \boldsymbol{x_{hd}} \tag{25}$$

where F represents the feedback force given to human hand, calculated by the error $\boldsymbol{e_f}$ between the MP control objective and the system final state. m_f, b_f, and k_f denote the inertia, damping, and stiffness parameters, respectively.

IV. Experiment

To verify the effectiveness of the proposed safety-enhanced shared control method, a series of experiments have been conducted both on simulation platforms and real experimental platforms.

A. Experimental setup

The human interacts with *sigma*.7 haptic device in a simulation environment conducted by *chai3d* framework, as shown in Fig. 3(a). To facilitate experimental operations, real-time refreshing screens of the front view and top view images are added to the simulation environment. Human can move the white ball freely in the absence of robot assistance (such as adjust the trajectory, obstacle avoidance, suspended and so on), and human also can accurately perform planned trajectory (red line) tracking with the assistance of robot. Fusion position (green ball) is the final state of our system. While without robot assistance, the fusion position is generally close to the haptic position. While within robot assistance, the fusion position is generally close to the planned trajectory. The distance between haptic actual position and the motion fusion control output will be sent to the human hand through the *sigma*.7 haptic device.

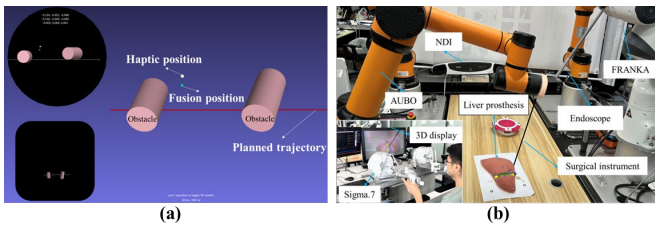

(a) (b)

Fig. 3: (a) The simulation experiment designed by chai3d. (b) The experimental master-slave surgical robot platform.

The master-slave surgical robot platform was self-developed by authors, as shown in Fig. 3(b). The main hardware included: a force dimension device, a 3D display, a computer, an NDI, a binocular endoscope, an electric coagulation rod, a switch, and two robot arms. The optical tracking system NDI (Polaris Vega XT) is used to unify the coordinate system and calibrate the rotation matrix from the robot's end to the surgical instrument's end. The endoscope clamped by the arm robot (FRANKA) is used to capture operation images and display them on the 3D display. The robot arm (AUBO i5) is used to clamp surgical instrument and connect to Sigma.7 realizing master-slave control and force feedback.

B. *Simulation result*

In the simulation section, the Fig. 4(a1-a3) illustrate the procedure of cutting under different velocity threshold scenarios: $v_0 = 0.5\,mm/s$, $v_0 = 1.0\,mm/s$, and $v_0 = 1.5\,mm/s$. The planned trajectory (red line) consisted of the predetermined planned waypoints drawn by a surgeon, the hand motion trajectory (blue line) data are collected from the haptic device, the green line denotes the motion fusion trajectory of the shared control method. Fig. 4(b1-b3) illustrate the velocity changes of human hand during the procedure of cutting. In Fig. 4(c1-c3), the green line denotes the errors between fusion trajectory and planned trajectory, and the blue line denotes the errors between fusion trajectory and hand trajectory, the red line is a baseline with $d_0 =$ 1.0 mm, which denotes the radius of the guiding channel. Fig. 4(d1-d3) illustrate the force feedback values of F_x, F_y, and F_z, calculated by the discrepancy between human control output and fusion control output. Fig. 4(e1-e3) illustrate the proportion of human and robot control evaluation gradient, the black area denotes control by human position tracking, the gray area denotes control by human velocity tracking, and the white area denotes control by robot assistance. In all pictures, the box area of A denotes that the operator is required to move quickly along the planned trajectory, the box area of B1 and B2 denotes that the operator actively perform obstacle avoidance tasks, the box area of C denotes that the operator actively simulated shaking and external collisions, the box area of D denotes that the operator actively terminate the operation task.

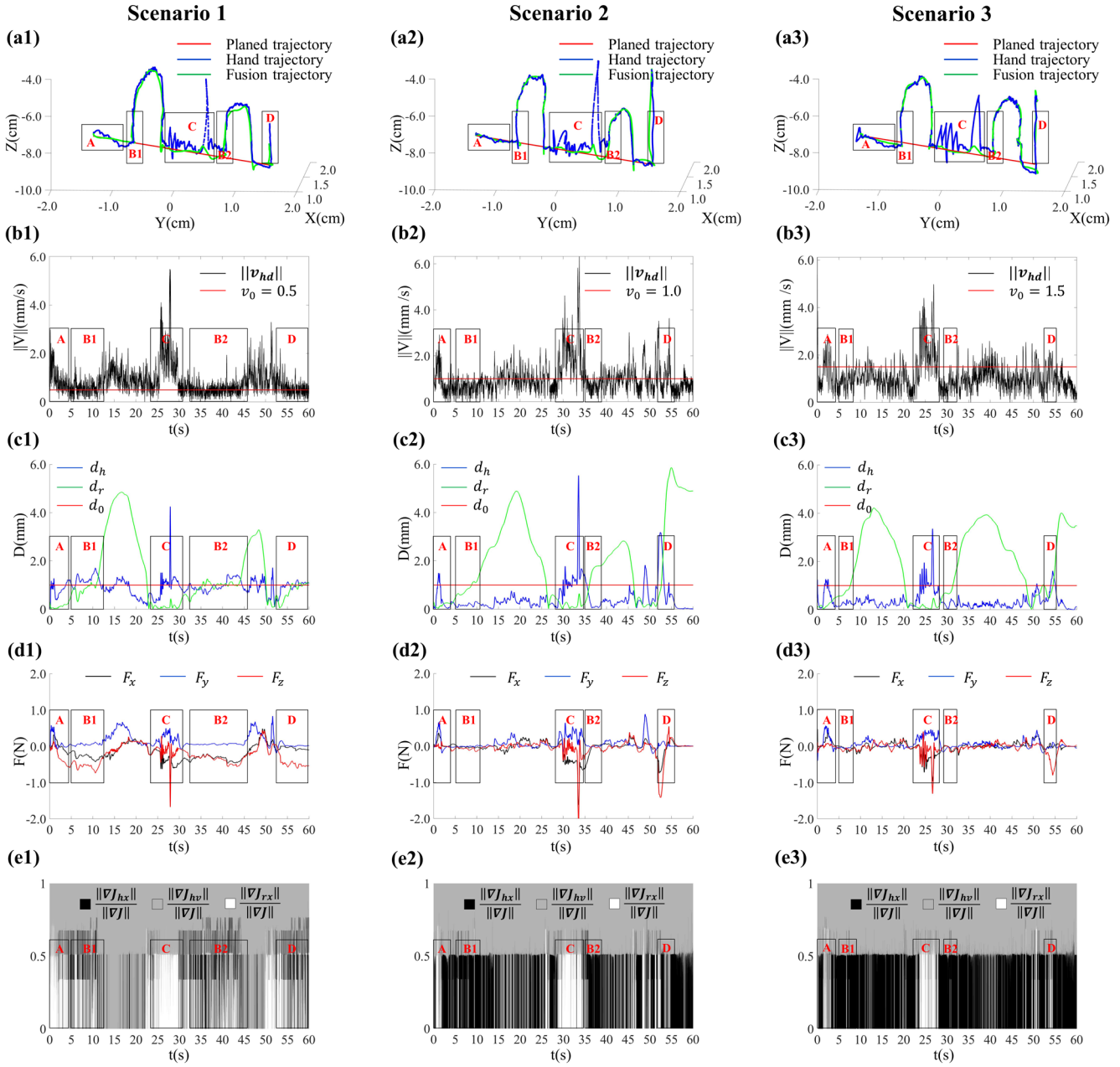

Fig.4: Comparison simulation results under different velocity threshold scenarios. (a) Cartesian trajectory tracking by integrating three controllers. (b) The magnitude of master hand velocity. (c) The errors between fusion trajectory and planned trajectory, and the the errors between fusion trajectory and hand trajectory (d) The force feedback values set to haptic device. (e) The stacked area chart illustrates the allocation of control authority between three controllers.

Firstly, to verify the precision of the robot-assisted cutting, the operator is required to move quickly along the planned trajectory as shown in the area A of Fig. 4(a1-a3). The average errors d_r between fusion trajectory and planned trajectory for the three scenarios are 0.07mm, 0.11mm, and 0.16mm respectively. From Fig. 4(a1-a3), it can be observed that the fused green line can more accurately fit the planned trajectory, but as the speed threshold v_0 increases, the precision cutting performance of robot-assisted cutting decreases. Overall, increasing hand velocity to trigger robot assistance has been proven to be a feasible approach, and can reduce the deviation error of the hand by approximately 0.66mm, as shown in Fig. 4(c1-c3).

Secondly, the operator can regain control by reducing the hand velocity at any time. As shown in Fig. 4(a1-a3), the operator can actively perform obstacle avoidance tasks in the areas of B1 and B2. However, by comparing graphs c1-c3, it can be observed that in the areas of B1 and B2, the errors d_h between the hand trajectory and the fusion trajectory are significantly greater in scenario 1. Similarly, the force values of F_x and F_z are significantly greater in scenario 1 in the areas of B1 and B2 compared to scenarios 2 and 3. This indicates that while setting a speed threshold too low can make it easier for the operator to obtain robot assistance, it can also result in frequent intervention from the robot and disrupt the operation of the human hand.

Thirdly, this mechanism has the potential to effectively filter out some hand tremors or non-subjective error operations. As shown in Fig. 4(a1-a3), the operator actively simulated shaking and external collisions during the operation in the areas of C, and the results showed that the fusion trajectory did not deviate significantly from the planned trajectory. Similarly, from the Fig. 4(c1-c3) in the areas of C, it can be observed that the errors in the deviation of the human hand trajectory is larger than the errors in the fusion trajectory. Moreover, the force feedback mechanism in this case also demonstrates the ability to allow the operator to become aware of some intentional operations, as shown in Fig. 4(d1-d3), the force opposite to the movement of the hand is applied to the hand device.

Finally, we present the allocation of control authority between three controllers in a stacked area chart depicted in Fig. 4(e1-e3). When $\|\boldsymbol{v_{hd}}\| < v_0$, the penalty function P_{rv} reduces J_{rx} to limit the robot's assistance capability. Similarly, when the fused trajectory deviates from the guiding channel ($d_r > d_0$), the penalty function P_{rx} limits the robot's assistance capability. As shown in Fig. 4(e3), during the obstacle avoidance progress, the white area disappears in the areas of B1 and B2. Moreover, as the v_0 increases, the robot's assistance becomes difficult to be triggered, so white areas in Scenario 3 are less than Scenario 1. On the other hand, when $\|\boldsymbol{v_{hd}}\| > v_0$, the penalty function P_{hx} reduces J_{hx} to reduce the accuracy of hand position tracking. And the operation is jointly controlled by hand velocity and robot assistance controller, which can eliminate hand tremors, avoid erroneous operations, and improve cutting accuracy. Additionally, the total area of the gray area and the black area remains greater than white areas at each time, indicating that in our shared control method, human control always maintains a dominant position.

C. *Experimental results*

In the real experiment, the operator completed a cutting process within 30 seconds, and the velocity threshold is set as $v_0 = 1.0$ mm/s and the radius of the guiding channel is set as $d_0 = 1.0$ mm. The operation process includes robot assistance in the box A, human active obstacle avoidance in the box B, human hand tremors in the box C and deliberate cessation in the box D, as shown in Fig. 5.

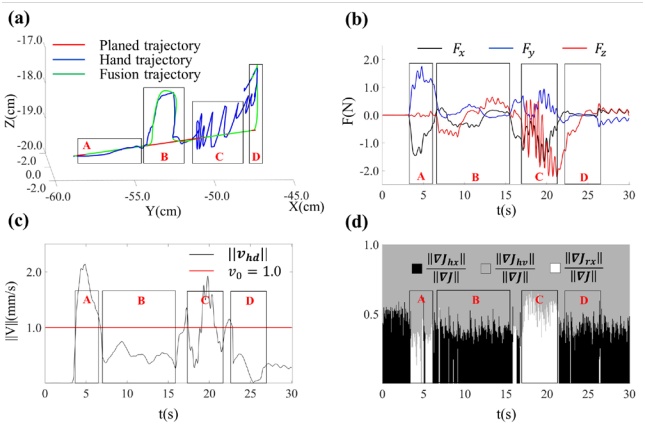

Fig.5: The experimental results. (a) Cartesian trajectory tracking by integrating three controllers. (b) The force feedback values set to haptic device. (c) The magnitude of master hand velocity. (d) The stacked area chart illustrates the allocation of control authority between three controllers.

As can be seen from the Fig.5(a), when $\|\boldsymbol{v_{hd}}\| > v_0$, high-efficiency robot assistance can be achieved in the box A and C, and both hand tremors and aberrant actions are also effectively mitigated. When $\|\boldsymbol{v_{hd}}\| < v_0$, the operator can adjust the cutting trajectory freely, accomplishing some active actions, for example obstacle evasion in the box B and deliberate cessation in the box D. The gray area in Fig.5(d) remains greater than white area, indicating that the human remains the leader during the whole procedure. As shown in Fig.5(b) effective tactile forces have been fed back to human hand in the box A and C and improve the safety of control.

V. Conclusion

This work proposed a safety-enhanced shared control for surgical assisted cutting based on position-velocity-force integration. The intelligent dynamic switching of autonomous scenarios and controllers can be realized through a motion fusion mechanism. And the novel allocation of control authority between three controllers can't deprive the surgeon of control authority during the operation. On the aspect of safety enhancement, the results shows that this method has the potential to effectively filter out some hand tremors and accidental operations, and the force feedback mechanism actually assist the surgeon in discerning the divergence between human hand actual position and the motion fusion control output. In conclusion, the proposed method shows good capabilities in human-robot shared control tasks, ensures the controllability, safety, transparency, and adaptability of the surgical robot system. Future works will apply this method to more complex surgical operation, and more intelligent controllers will be introduced to verify the performance of human-robot integration.

REFERENCES

[1] G.-Z. Yang *et al.*, "Medical robotics—Regulatory, ethical, and legal considerations for increasing levels of autonomy," *Sci. Robot.,* vol. 2, p. eaam8638, 2017.

[2] K. A. Nichols and A. M. Okamura, "A Framework for Multilateral Manipulation in Surgical Tasks," *IEEE Transactions on Automation Science and Engineering,* vol. 13, no. 1, pp. 68-77, 2016.

[3] D. A. Abbink *et al.*, "A Topology of Shared Control Systems—Finding Common Ground in Diversity," *IEEE T. Hum.-Mach. Syst.,* vol. 48, no. 5, pp. 509-525, 2018.

[4] D. A. Abbink, M. Mulder, and E. R. Boer, "Haptic shared control: smoothly shifting control authority?," *Cognition, Technology & Work,* vol. 14, no. 1, pp. 19-28, 2012.

[5] R. Parasuraman and V. Riley, "Humans and Automation: Use, Misuse, Disuse, Abuse," *Human Factors,* vol. 39, no. 2, pp. 230-253, 1997.

[6] M. Dominici and R. Cortesão, "Cascade robot force control architecture for autonomous beating heart motion compensation with model predictive control and active observer," *Proceedings of the IEEE RAS and EMBS International Conference on Biomedical Robotics and Biomechatronics,* pp. 745-751, 2014.

[7] M. Dominici and R. Cortesão, "Model predictive control architectures with force feedback for robotic-assisted beating heart surgery," in *2014 IEEE International Conference on Robotics and Automation (ICRA)*, pp. 2276-2282, June 2014.

[8] Y. Nakamura, K. Kishi, and H. Kawakami, "Heartbeat synchronization for robotic cardiac surgery," in *Proceedings 2001 ICRA. IEEE International Conference on Robotics and Automation (Cat. No.01CH37164)*, vol. 2, pp. 2014-2019, May 2001.

[9] R. Cortesao and M. Dominici, "Robot Force Control on a Beating Heart," *IEEE-ASME Trans. Mechatron.,* vol. PP, no. 4, pp. 1-1, 2017.

[10] L. Zheng, H. Wu, L. Yang, Y. Lao, Q. Lin, and R. Yang, "A Novel Respiratory Follow-Up Robotic System for Thoracic-Abdominal Puncture," *IEEE Trans. Ind. Electron.,* vol. 68, no. 3, pp. 2368-2378, 2021.

[11] M. Selvaggio, G. Fontanelli, F. Ficuciello, L. Villani, and B. Siciliano, "Passive Virtual Fixtures Adaptation in Minimally Invasive Robotic Surgery," *IEEE Robot. Autom. Lett.,* vol. PP, pp. 1-1, 06/22 2018.

[12] L. Xiong, C. B. Chng, C. K. Chui, P. Yu, and Y. Li, "Shared control of a medical robot with haptic guidance," *International Journal of Computer Assisted Radiology and Surgery,* vol. 12, no. 1, pp. 137-147, 2017.

[13] C. Lauretti, F. Cordella, C. Tamantini, C. Gentile, F. S. d. Luzio, and L. Zollo, "A Surgeon-Robot Shared Control for Ergonomic Pedicle Screw Fixation," *IEEE Robot. Autom. Lett.,* vol. 5, no. 2, pp. 2554-2561, 2020.

[14] R. Rahal, F. Abi-Farraj, P. R. Giordano, and C. Pacchierotti, "Haptic Shared-Control Methods for Robotic Cutting under Nonholonomic Constraints," in *2019 IEEE/RSJ International Conference on Intelligent Robots and Systems (IROS)*, 3-8, pp. 8151-8157, 2019.

[15] Y. He, Y. Hu, P. Zhang, B. Zhao, X. Qi, and J. Zhang, "Human–Robot Cooperative Control Based on Virtual Fixture in Robot-Assisted Endoscopic Sinus Surgery," *SN Appl. Sci.,* vol. 9, p. 1659, 2019.

[16] G. A. Fontanelli, G. Z. Yang, and B. Siciliano, "A Comparison of Assistive Methods for Suturing in MIRS," in *2018 IEEE/RSJ International Conference on Intelligent Robots and Systems (IROS)*, pp. 4389-4395, Oct. 2018.

[17] X. Ma, P. Wang, M. Ye, P. W. Y. Chiu, and Z. Li, "Shared Autonomy of a Flexible Manipulator in Constrained Endoluminal Surgical Tasks," *IEEE Robot. Autom. Lett.,* vol. 4, no. 3, pp. 3106-3112, 2019.

[18] O. Wilz, B. Sainsbury, and C. Rossa, "Constrained haptic-guided shared control for collaborative human–robot percutaneous nephrolithotomy training," *Mechatronics.,* vol. 75, p. 102528, 2021.

[19] P. L. Yen and T. H. Ho, "Shared Control for a Handheld Orthopedic Surgical Robot," *IEEE Robot. Autom. Lett.,* vol. 6, no. 4, pp. 8394-8400, 2021.

[20] R. Moccia, M. Selvaggio, L. Villani, B. Siciliano, and F. Ficuciello, "Vision-based Virtual Fixtures Generation for Robotic-Assisted Polyp Dissection Procedures," in *2019 IEEE/RSJ International Conference on Intelligent Robots and Systems (IROS)*, pp. 7934-7939, Nov. 2019.

[21] M. Selvaggio, A. Ghalamzan, R. Moccia, F. Ficuciello, and B. Siciliano, "Haptic-guided shared control for needle grasping optimization in minimally invasive robotic surgery," *IEEE/RSJ International Conference on Intelligent Robots and Systems,* 2019.

[22] M. M. Marinho, H. Ishida, K. Harada, K. Deie, and M. Mitsuishi, "Virtual Fixture Assistance for Suturing in Robot-Aided Pediatric Endoscopic Surgery," *IEEE Robot. Autom. Lett.,* vol. 5, no. 2, pp. 524-531, 2020.

[23] N. Sayols *et al.*, *Global/local motion planning based on Dynamic Trajectory Reconfiguration and Dynamical Systems for Autonomous Surgical Robots*, pp. 8483-8489, 2020.

[24] M. M. Marinho, B. V. Adorno, K. Harada, and M. Mitsuishi, "Dynamic Active Constraints for Surgical Robots Using Vector-Field Inequalities," *IEEE Trans. Robot.,* vol. 35, no. 5, pp. 1166-1185, 2019.

[25] H. Qiu, B. Pan, Y. Fu, and Y. Ai, "Surgical Instruments Motion Safety Constraint Based on Haptic Virtual Fixture," in *2019 IEEE International Conference on Mechatronics and Automation (ICMA)*, pp. 2267-2272, Aug. 2019.

[26] Y. Li, K. P. Tee, W. L. Chan, R. Yan, Y. Chua, and D. K. Limbu, "Continuous Role Adaptation for Human–Robot Shared Control," *IEEE Trans. Robot.,* vol. 31, no. 3, pp. 672-681, 2015.

[27] H. Saeidi, J. D. Opfermann, M. Kam, S. Raghunathan, S. Leonard, and A. Krieger, "A Confidence-Based Shared Control Strategy for the Smart Tissue Autonomous Robot (STAR)," in *2018 IEEE/RSJ International Conference on Intelligent Robots and Systems (IROS)*, pp. 1268-1275, Oct. 2018.

[28] H. Su, W. Qi, Y. Schmirander, S. E. Ovur, S. Cai, and X. Xiong, "A human activity-aware shared control solution for medical human–robot interaction," *Assembly Automation,* vol. 42, no. 3, pp. 388-394, 2022.

[29] P. Franceschi, N. Pedrocchi, and M. Beschi, "Adaptive Impedance Controller for Human-Robot Arbitration based on Cooperative Differential Game Theory," in *2022 International Conference on Robotics and Automation (ICRA)*, , pp. 7881-7887, May. 2022.

[30] D. Zhang *et al.*, "Human-Robot Shared Control for Surgical Robot Based on Context-Aware Sim-to-Real Adaptation," in *2022 International Conference on Robotics and Automation (ICRA)*, pp. 7694-7700, May 2022.

[31] R. Chipalkatty, G. Droge, and M. B. Egerstedt, "Less Is More: Mixed-Initiative Model-Predictive Control With Human Inputs," *IEEE Trans. Robot.,* vol. 29, no. 3, pp. 695-703, 2013.